Original Research Article

Nonlinear FE Prediction of Shear Strength of RC T-Beams with flange in compression zone

Abstract: This research aims at the theoretical prediction of the shear strength of reinforced concrete T-beams when the flange is **subjected to compression stresses**. This objective was accomplished by means of specially developed nonlinear FE models that are first verified using experimental results. The 3-D nonlinear models of flanged beams were performed using the ANSYS V-19.2 program [1]. To validate the proposed FE model, its results were compared to specially designed and conducted experiments that included beams with variable flange dimensions (width and depth). Results of the FE models agreed very well with their corresponding experimental results in terms of characterized loads and deflections (ratio ranged between 0.87 and 1.03). The theoretical and experimental crack patterns were also similar.

Then, the FE model is applied in an extensive parametric study. Ninety-seven beam models were analyzed as simply supported under the effect of two concentrated point loads (four-point load configuration). The structural performance of flanged beams was investigated from zero load up to failure. Four parameters were examined: flange dimensions (width and depth); longitudinal reinforcement in flange; concrete compressive strength "f_c'"; and shear span to depth ratio. Results of flanged beams were compared to those of a similar beam without flanges considered as the reference or control case. For the tested parameters and within the examined range, presence of flanges in T-beams increased the shear strength by up to 260% of the shear strength of the web alone. Shear strength of flanged beams increased directly with the increase in flange dimensions where the effect of flange thickness was more pronounced than effect of flange width. Besides, presence of longitudinal reinforcement in the flange enhanced the beam shear strength by up to 40%, compared to beams without flange reinforcement. Moreover, for various beam conditions, the shear strength increased to about three folds when the shear span to depth ratio was reduced from 2.0 to 0.5.

Keywords: finite element analysis, shear strength, reinforced concrete beams, T-beam, Girder.

1. Introduction

Flanged reinforced concrete beams have been widely used in many applications in the field of civil engineering. As such, the performance of these structural members was discussed experimentally as well as analytically. Hesham et al. [2] conducted a numerical experimental study the shear behavior of lightweight concrete flanged beams. Six lightweight concrete beams were tested to investigate the effects of flange width and shear span to depth ratio. Their experimental and FE results showed that the failure load of T-beams with different flange widths (320, 520, and 720 mm) increased in proportion to the flange width. However, it was also observed that the failure load was inversely proportional to all the shear span to depth ratio.

Balamuralikrishnan et al. [3] performed experiments as well as FE investigations to evaluate the performance of RC T-beams reinforced internally with GFRP reinforcements to shearing loads. A total of twelve specimens were tested with varying parameters (type of reinforcements, reinforcements ratio, and concrete grade). Finite element modeling of the T-beams was done using ANSYS program utilizing two special elements: solid 65 and link 8. The experimental outcomes of the flanged beams agreed well with the FE numerical results.

Hamdy et al. [4] showed that finite element modeling via ANSYS program was able to fairly predict the performance of RC T-beams with openings reinforced with either carbon fiber reinforced polymer (CFRP) or basalt fiber reinforced polymer (BFRP) sheets. In particular,

ANSYS finite element models could reasonably predict the failure load and the mode of failure for the analyzed beams.

Hugo et al. [5] pointed out that the serviceability circumstances of T-beams can be improved by increasing the concrete strengths as concrete strength has an essential influence on the de-bonding phenomenon.

Pansuk et al. [6] indicated that an increase in the flange width of a T-beam gave higher shear capacity (in a nonlinear relationship) for the T-beams with shear reinforcement. However, they found that in the case of a T-beam without shear reinforcement, the width of the flange has almost no effect on shear capacity.

Sato et al. [7] showed that concrete top flanges had significant effects on shear behavior of RC T-beams as it affects the shear strength, stress in shear reinforcement, and crack propagation. Concrete top flanges could also reduce the shear strains in the beam web. They recommended that concrete top flange near compression zone should be considered as part of the shear resisting mechanism of T-beams.

Finally, Giaccio et al. [8] tested fifteen flanged specimens with shear reinforcement and web longitudinal reinforcement. There observed the effect of the flange width to web width ratio (b_f/b_w) on the shear strength of reinforced concrete T-beams; this effect depended on the ratio of flange thickness to effective beam depth (d_f/d_o). They suggested based on their experiments that as long as the ratio d_f/d_o is above a certain minimum value ($d_f/d_o \geq 0.25$), then the increase in shear resistance for a given increase in b_f/b_w is independent of d_f/d_o.

Numerical analysis technique that is based on the finite element method has been checked in this research to detect the effect of the flange on the reinforced concrete T-beams in both pre- and post-cracking stages of loading and up to ultimate load. ANSYS [1] is adopted in the study as it is furnished with sufficient modelling features that suit the finite

element analysis of RC beams. First, 3-D nonlinear FE models of flanged beams "***with flange in the compression***" were specially developed using ANSYS V-19.2. Then, results obtained were validated through comparisons with the test results of specially designed and conducted experiments that included similar beams. Results of the FE models agreed very well with th corresponding experimental results; the theoretical and experimental crack patterns were also in good practical agreement. Using this validated model, it was possible to run an extensive parametric study of all variables, a study that couldn't be done experimentally due to cost and time constraints.

2. Finite Element Modeling Using ANSYS

2.1. Geometry

Finite element modeling and nonlinear analysis are performed using ANSYS software. The structural element types adopted for geometric idealization of the different materials are SOLID 65 for concrete, and LINK 8 for steel bars and stirrups. In order to avoid stress concentration problems such as localized crushing of concrete elements near the bearing and loading plates, SOLID 45 elements are used to model the 30 mm thickness steel plates inserted at locations of supports and concentrated loads (see Fig. 1 for modelling layout). For solving the nonlinear equations using Newton- Raphson equilibrium iteration technique, the infinite norm of displacement and the convergence precision are taken equal to 0.05 [9,10,11]. Figure 2 shows the loading configuration and support conditions.

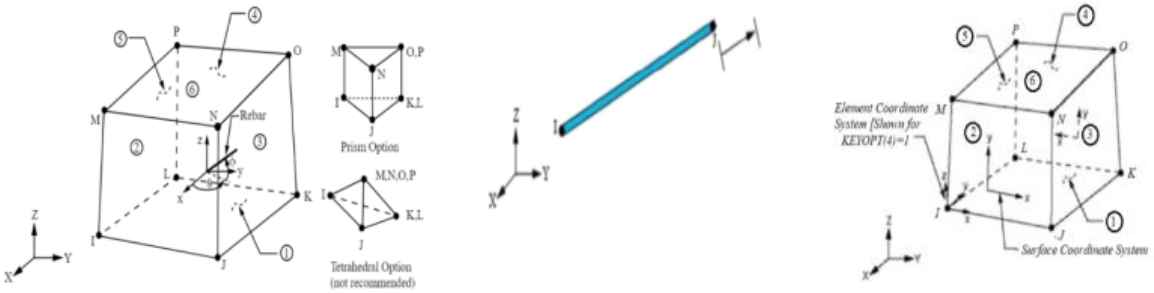

(a) Solid 65 (b) Link 8 (c) Solid 45

Fig. 1. Structural elements idealization for the numerical models [9].

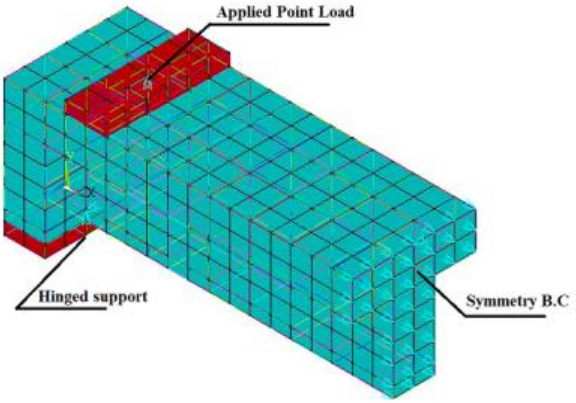

Fig. 2. Applied Load and Support Conditions.

2.2. Constitutive Relations

Constitutive relationships for both the reinforcement and the concrete are described below.

2.2.1. Constitutive relation for concrete

Concrete is a quasi-brittle material that behaves differently in compression and tension. The tensile strength of concrete is typically 8-15% of its compressive strength [12]. Figure 3 shows a typical stress-strain curve for normal weight concrete applied in our numerical study [13].

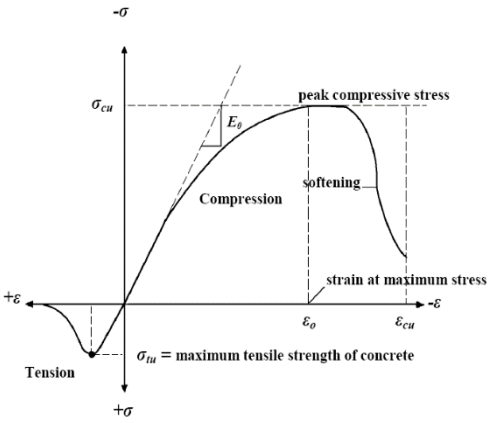

Fig. 3. Typical uniaxial compressive and tensile stress-strain curve for concrete (Bangash1989)

To define concrete material in ANSYS, the following inputs are required: elastic modulus (E_c); ultimate uniaxial compressive strength (f'_c); ultimate uniaxial tensile strength (modulus of rupture, f_r); Poisson's ratio (v); and shear transfer coefficient (β_t). To define the uniaxial stress-strain relationship for concrete in compression, Eqs. 1 to 3 were used [14].

$$f = \frac{E_c \varepsilon}{1+\left(\frac{\varepsilon}{\varepsilon_o}\right)^2} \quad (1)$$

$$\varepsilon_o = \frac{2f_c`}{E_c} \quad (2)$$

$$E_c = \frac{f}{\varepsilon} \quad (3)$$

Where:

f = stress at any strain ε, psi
ε = strain at stress f
ε_o = strain at the ultimate compressive strength f_c'
E_c = the initial tangent modulus for concrete in MPa and is defined according to ACI-318 14 [17] by the following equations:

$$E_c = 4700\sqrt{f_c`} \quad (4)$$

Figure 4 shows the simplified compressive uniaxial stress-strain relationship adopted in this study.

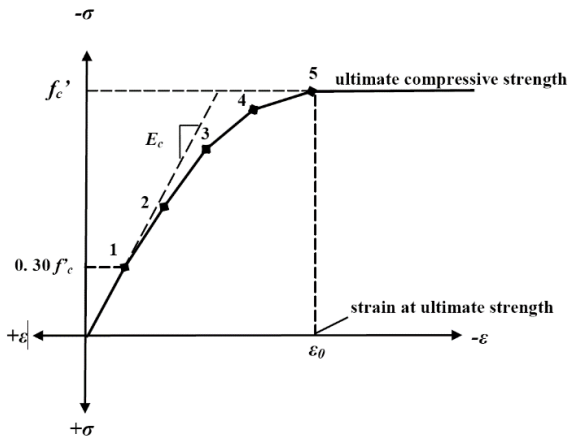

Fig. 4. Simplified compressive uniaxial stress-strain curve for concrete

2.2.2. Constitutive relation for steel

Figure 5 shows the idealized stress-strain relationship for the steel reinforcement. Material properties are as follows: elastic modulus, E_s=200,000 MPa; yield stress, f_y = 420 MPa (Lab test); and Poisson's ratio, v = 0.3.

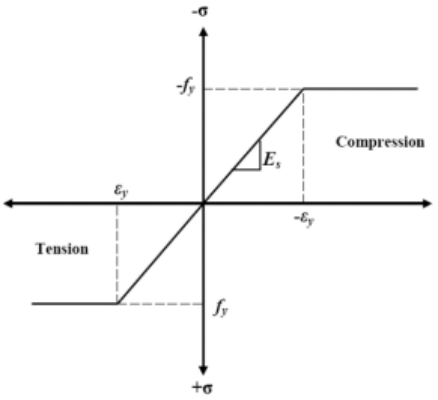

Fig.5. Idealized stress-strain curve for reinforcing steel

3. Model Validation

In this section, results of the FE model are validated using test results of a recent experimental investigation conducted by the authors [16]. Table 1 presents the geometrical and mechanical properties of few selected specimens for comparison. Further, the test set-up together with specimens' details are shown in Figures 6 and 7, respectively, while the corresponding finite element models are shown in Fig. 8. For details about the full experimental program which included nineteen specimens, please refer to [16].

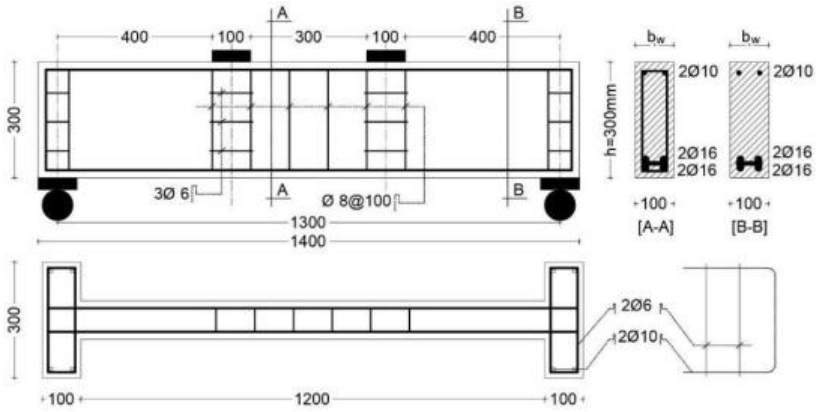

[a]- Specimen with Rectangular cross section (control)

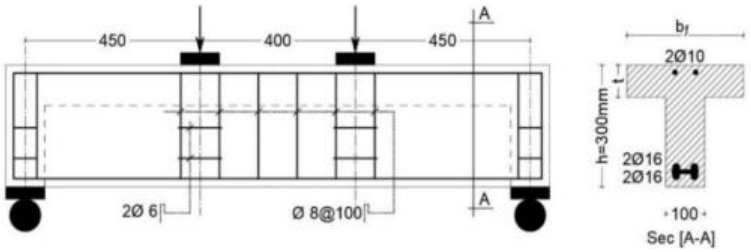

[b]- T- cross section without stirrups

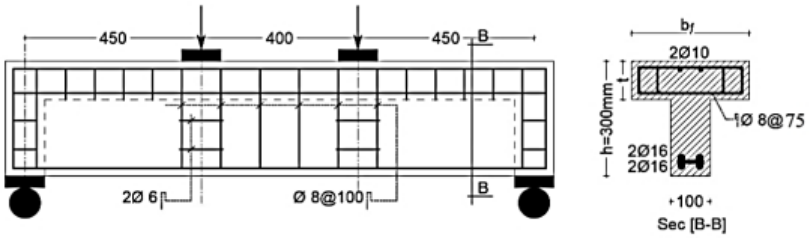

[c]- T- cross section with stirrups

Fig. 6. Specimen details and arrangement of reinforcement (All dimensions in mm) [16]

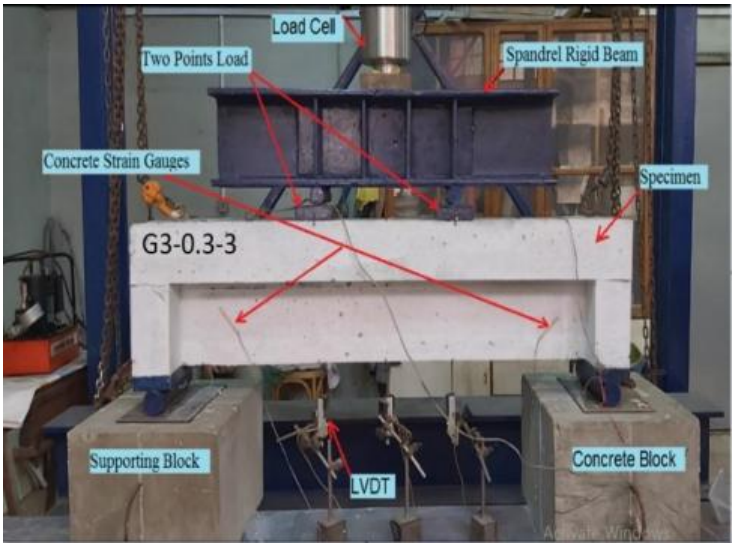

Fig. 7. Preparation of Test Set-up Specimens [**16**]

[Table-1] Experimental Program

Specimen	Cross Sectional (Area (cm^2	Cross Sectional Area Increasing (%)	.Flange Dim			Stirrups in flange within shear zone (mm)	Longitudinal reinforcement in Flange		Longitudinal reinforcement in Flange [%]
			t_f (cm)	b_f ((cm	A_f ((cm^2		Bottom Steel	Top Steel	
C0	300	------			------	------		------	------
G1-0.3-3	480	60%	0.3h= 9	30	270	------		------	------
G3-0.5-5	900	200%	0.5h=15	50	750	Ø8@75	+ Ø 10 6 1Ø10/side	Ø 8 + 2 Ø 2 6	1.046%

For specimens G1-0.3-3 and G3-0.5-5: the first part G1 refers to without flange reinforcement while G3 with longitudinal bars and flange stirrups within the shear zones; the second part refers to the ratio of flange thickness to the total depth (ρ_t = 0.3 and 0.5); and the third part refers to the flange width to web width ratio (ρ_b = 3 and 5).

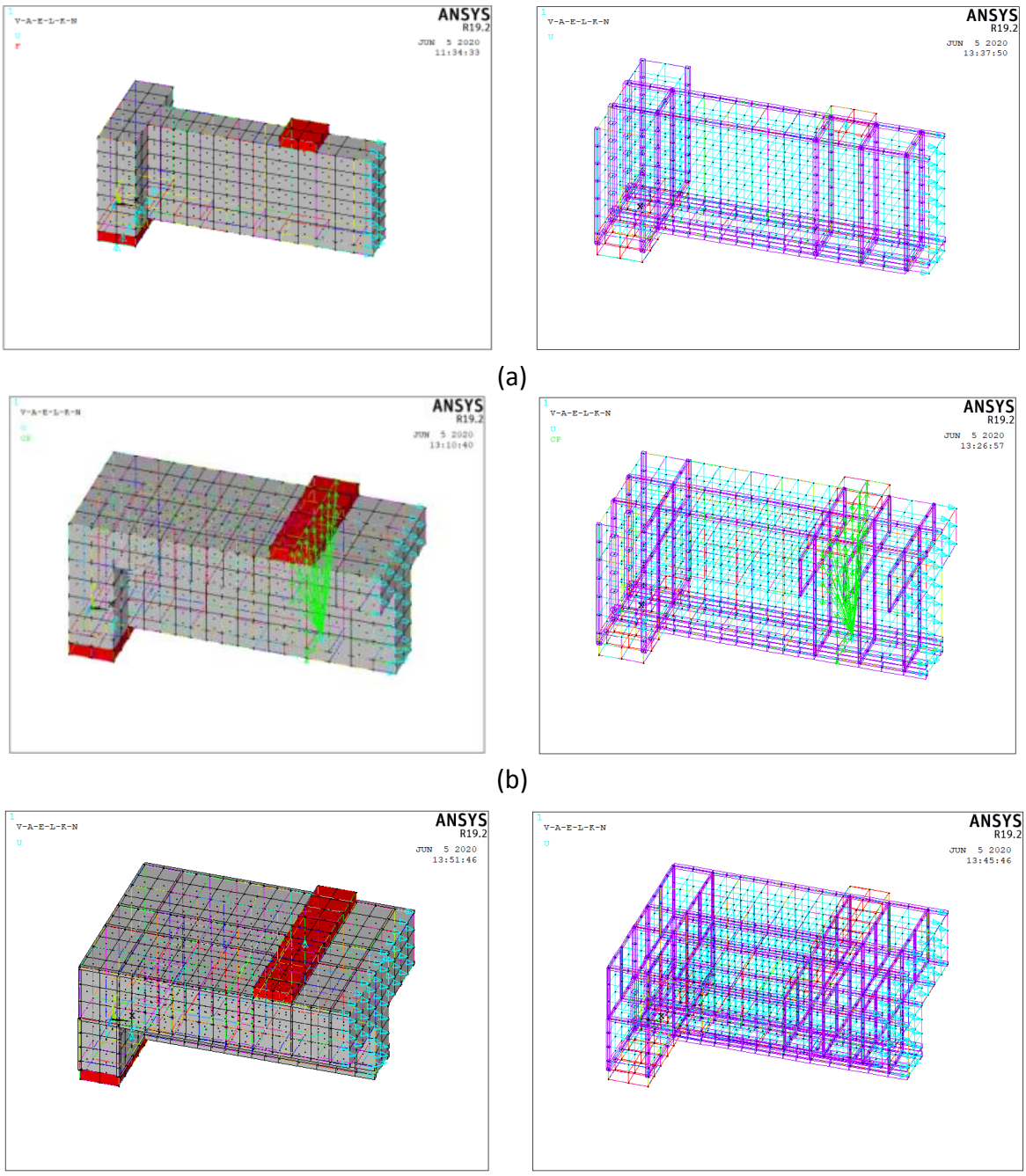

Fig. 8. Finite Element Simulation Models for specimens: a) Rectangular; b) G1-0.3-3; and c) G3-0.5-5 from Ref. [16]

3.1. Load deflection curves

Figure 9 compares the load-deflection calculated using ANSYS models with th corresponding experimental measurements for three specimens (C0, G1-0.3-3 & G3-0.5-5). It is seen that the FE results agree very well with the experiments [16] in terms of the ultimate load capacity (P_u) and the corresponding ultimate deflection (Δ_u). It is noted,

however, that- in the initial part- the theoretical load-deflection curve is 9% to 15% stiffer than that obtained experimentally. Besides, the average ratio of FE to experimental ultimate deflections [$\Delta_{u(FE)}/\Delta_{u(EXP)}$] for all specimens was 0.87.

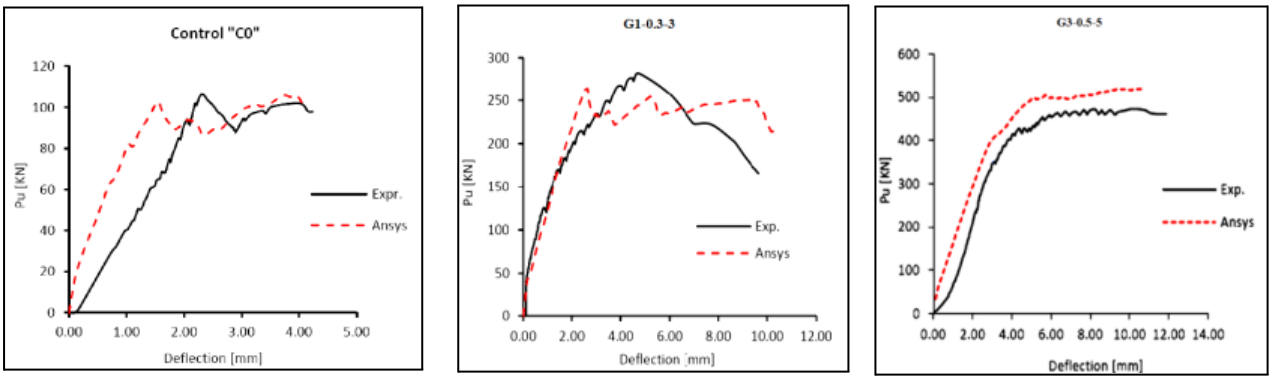

(a) (b) (c)

Fig.9. Predicted and Measured Load-Deflections Curves for Three Specimens: a) Rectangular; b) G1-0.3-3; and c) G3-0.5-5. [16]

3.2. Ultimate load comparison

The experimental ultimate l for specimens C0, G1-0.3-3, and G3-0.5-5 w 106.4, 281.9, and 473.8 kN; respectively; while its FE predictions were 113.4, 264.1, and 516.2 kN; respectively. The difference between the theoretical and experimental ultimate loads is about ±6%, while the average of the [$Pu_{(FE)}$ / $Pu_{(EXP)}$] ratio for all specimens is 1.03. This validates accuracy of the ANSYS model and qua it for use in the parametric study to examine the performance of reinforced concrete T-beams.

3.3. Crack pattern and failure mode

A comparison between the experimental crack patterns for tested beams in Ref. [16] with the predicted crack patterns by ANSYS is shown in Fig. 10. All specimens failed in shear mo distinguished by wide diagonal cracks extending from close to the supporting column

towards the steel loading plate. In addition, the figure shows change in spreading of cracks with the presence and size of flange.

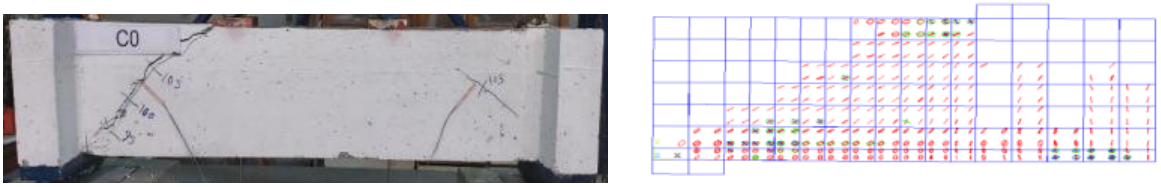

P_u=106 kN P_u=113.4 kN

(a)

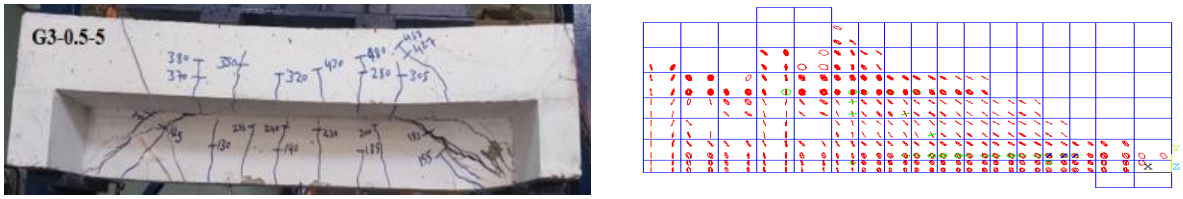

P_u=281.9 kN P_u=264.1 kN

(b)

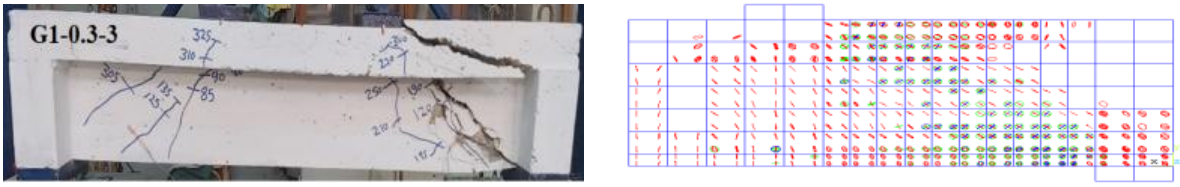

P_u=473.8 kN P_u=516.2 kN

(c)

Fig. 10. Predicted and Observed Cracking Patterns and Failure Load for Three Specimens: a) Rectangular; b) G1-0.3-3; and c) G3-0.5-5 [16].

4. Parametric study.

4.1. General

To study the effect of different parameters on the structural response of RC T-beams, several beams (labeled as S, S1, S2, ... S96) are analyzed. As given in Table 2, the main considered parameters include: (1) the concrete strength (fc'), (2) width ratio (ρ_b), (3) depth ratio (ρ_t), (4) ratio of longitudinal steel in flange (ρ), and (5) shear span to depth ratio (a/d). The rectangular beam S is the reference or control case.

Table 2 Parametric Study

Specimen	width ratio (ρ_b)	depth ratio (ρ_t)	*a/d*	$f_{c'}$	*Longitudinal steel in flange* ρ %	*No of Runs*
S	------	------	2.0	30	-----	1
S 1:12	3	0.10, 0.3, 0.5& 0.7	0.5, 1.0, and 2.0	30	0.5	12
S 13:24	5	0.10, 0.3, 0.5& 0.7	0.5, 1.0, and 2.0	30	0.5	12
S 25:48	7	0.10, 0.3, 0.5& 0.7	0.5, 1.0, and 2.0	30 and 60	0.5	24
S 49:84	7	0.10, 0.3, 0.5& 0.7	0.5, 1.0, and 2.0	30	0.0, 1.0, and 2.0	36
S 85:96	9	0.10, 0.3, 0.5& 0.7	0.5, 1.0, and 2.0	30	0.5	12
					Total	97

Width ratio ($\rho_b = b_f/b_w$) is the ratio of flange width "b_f "and web width "b_w ", depth ratio ($\rho_t = t/h$) is the ratio of flange thickness "t" and total web depth "h", *a/d* is the span to depth ratio, ρ % is the longitudinal steel in the flange. Control specimen S is rectangular section, with total depth 300 mm and width 100 mm.

Note: In every row of Table 2, as the beam label increases (from Si to Si+1, Si+2, etc.) changes in parameters occur first for ρ_t , then for *a/d,* then for $f_{c'}$, and finally for ρ, as listed in the table. Thus, S49 designates the beam with ρ_t =0.1, *a/d=0.5,* and ρ*=0.0*, while S54 represents the beam with ρ_t =0.3, *a/d=1.0,* and ρ*=0.0*, and S79 is the beam with ρ_t =0.5, *a/d=1.0,* and ρ*=2.0*.

4.2. Presentation of ANSYS results

Results are presented in terms of the following measures:

- Loads at the yield level (P_y) and at the ultimate level (P_u).
- Deflection at the yield level (Δ_y) and at the ultimate level (Δ_u).
- Displacement ductility (μ_Δ) = (Δ_u/Δ_y).
- Toughness (I) = the area under the load-deflection curve.

Table 3 Numerical results for various analyzed beams

Specimen	P_u *(kN)*	P_y *(kN)*	P_{cr} *(kN)*	Δ_u *(mm)*	Δ_y *(mm)*	Δ_{cr} *(mm)*	Q_{uR}	α_{uR}	*I*	I_{uR}
S	141.61	------	33.47	2.81	------	0.34	1	1	1089	1.0
S1	559.50	356.40	140.44	2.86	3.03	0.36	3.95	1.02	2907	2.7
S2	516.96	437.77	142.56	2.04	2.51	0.33	3.65	0.73	3846	3.5
S3	692.85	430.30	150.87	2.91	3.18	0.38	4.89	1.04	3673	3.4
S4	714.67	N.Y*	178.62	2.43	N.Y*	0.38	5.05	0.86	4364	4.0
S5	300.22	210.57	72.36	2.53	2.82	0.38	2.12	0.90	1717	1.6
S6	328.58	271.78	72.66	2.67	3.53	0.33	2.32	0.95	2715	2.5
S7	440.19	427.09	73.28	3.92	4.21	0.34	3.11	1.40	3104	2.9
S8	500.99	N.Y	86.67	3.65	N.Y	0.33	3.54	1.30	3119	2.9
S9	156.09	100.52	38.30	2.69	7.35	0.32	1.10	0.96	1022	0.9
S10	198.57	147.53	35.73	3.57	5.05	0.27	1.40	1.27	1446	1.3
S11	270.99	195.03	37.47	4.50	5.37	0.27	1.91	1.60	1674	1.5
S12	354.17	N.Y	45.78	5.13	N.Y	0.29	2.50	1.83	2127	2.0
S13	572.64	560.06	148.62	2.54	2.56	0.38	4.04	0.90	3088	2.8
S14	623.87	621.41	157.71	2.93	2.90	0.37	4.41	1.04	4861	4.5
S15	769.96	756.27	168.70	2.75	3.50	0.40	5.44	0.98	6633	6.1
S16	882.42	N.Y	218.41	2.86	N.Y	0.34	6.23	1.02	6909	6.3
S17	284.25	193.88	71.34	2.35	4.11	0.33	2.01	0.84	1883	1.7
S18	361.60	282.53	73.14	2.70	3.72	0.32	2.55	0.96	2871	2.6
S19	520.52	492.87	80.92	4.67	5.07	0.33	3.68	1.66	4373	4.0
S20	651.44	N.Y	110.52	4.23	N.Y	0.33	4.60	1.51	4493	4.1
S21	155.06	98.58	34.58	4.24	6.02	0.23	1.09	1.51	1087	1.0
S22	205.31	172.54	38.04	3.23	6.78	0.30	1.45	1.15	1540	1.4
S23	291.47	253.38	43.59	4.14	5.38	0.23	2.06	1.47	2194	2.0
S24	437.37	422.75	59.74	5.62	5.01	0.29	3.09	2.00	3605	3.3
S25	539.03	450.27	147.13	2.50	1.55	0.36	3.81	0.89	4428	4.1
S26	601.13	555.55	155.19	2.03	2.28	0.36	4.24	0.72	5587	5.1
S27	813.05	598.64	186.74	2.41	4.57	0.37	5.74	0.86	6426	5.9
S28	955.33	N.Y	266.28	2.51	N.Y	0.35	6.75	0.89	6911	6.3
S29	291.17	206.89	75.67	2.16	3.73	0.32	2.06	0.77	2055	1.9
S30	370.20	340.28	76.91	2.53	4.11	0.31	2.61	0.90	3413	3.1
S31	583.19	432.66	89.37	3.64	4.33	0.31	4.12	1.29	4434	4.1
S32	683.84	N.Y	140.99	3.85	N.Y	0.33	4.97	1.37	5042	4.6
S33	155.33	142.38	40.71	2.58	5.27	0.28	1.10	0.92	1172	1.1
S34	216.92	162.65	43.43	3.07	6.90	0.23	1.53	1.09	1683	1.5
S35	345.30	N.Y	48.58	4.41	N.Y	0.26	2.44	1.57	2678	2.5
S36	468.64	N.Y	73.43	4.76	N.Y	0.28	3.31	1.69	3403	3.1
S37	966.03	780.48	184.95	3.21	3.44	0.29	6.82	1.14	8841	8.1
S38	1160.45	1091.52	190.97	4.03	3.66	0.30	8.19	1.43	10419	9.6
S39	1616.71	1488.36	225.87	11.42	5.14	0.33	11.42	4.06	16049	14.7

Specimen	P_u (kN)	P_y (kN)	P_{cr} (kN)	Δ_u (mm)	Δ_y (mm)	Δ_{cr} (mm)	Q_{uR}	α_{uR}	*I*	I_{uR}
S40	1575.32	1409.87	337.32	4.47	8.56	0.33	11.12	1.59	12934	11.9
S41	537.98	457.99	88.35	3.81	5.05	0.33	3.80	1.35	4829	4.4
S42	729.11	674.25	94.84	15.30	7.70	0.31	5.15	5.44	9242	8.5
S43	899.35	830.58	113.21	17.34	6.49	0.31	6.35	6.17	13217	12.1
S44	1089.80	1010.36	178.46	12.49	5.27	0.33	7.70	4.44	14311	13.1
S45	291.42	258.80	43.89	5.41	7.07	0.27	2.06	1.93	2239	2.1
S46	387.44	362.88	46.12	11.57	6.76	0.26	2.74	4.12	3544	3.3
S47	471.56	420.76	57.63	11.46	5.11	0.26	3.33	4.08	4526	4.2
S48	594.53	515.21	93.98	12.00	4.23	0.28	4.20	4.27	5637	5.2
S49	552.96	N.Y	141.13	2.34	N.Y	0.33	3.90	0.83	4069	3.7
S50	618.56		155.58	2.23		0.29	4.37	0.80	5694	5.2
S51	772.52		157.25	2.73		0.25	5.46	0.97	5932	5.4
S52	831.80		184.54	2.95		0.24	5.87	1.05	7118	6.5
S53	305.85		102.28	2.40		0.60	2.16	0.85	2832	2.6
S54	340.13		76.79	2.35		0.31	2.40	0.84	1628	1.5
S55	456.24		87.24	3.21		0.30	3.22	1.14	3252	3.0
S56	648.25		135.01	5.25		0.35	4.58	1.87	5316	4.9
S57	161.20		37.59	2.66		0.27	1.14	0.95	1086	1.0
S58	229.81		39.64	3.93		0.27	1.62	1.40	1591	1.5
S59	310.08		46.74	5.56		0.27	2.19	1.98	2277	2.1
S60	336.09		65.19	6.74		0.26	2.37	2.40	3019	2.8
S61	545.20	435.37	146.33	2.21	9.09	0.36	3.85	0.79	4563	4.2
S62	673.43	N.Y	159.83	2.25	N.Y	0.39	4.76	0.80	5696	5.2
S63	839.89		188.97	2.51		0.33	5.93	0.89	6190	5.7
S64	972.73		254.32	2.45		0.31	6.94	0.87	8186	7.5
S65	319.21	216.90	78.21	2.47	9.33	0.37	2.25	0.88	2430	2.2
S66	418.11	N.Y	83.40	3.02	N.Y	0.37	2.95	1.07	3392	3.1
S67	610.65		91.59	4.44		0.30	4.31	1.58	5294	4.9
S68	703.74		151.69	3.51		0.34	4.83	1.25	5627	5.2
S69	155.78		40.91	2.50		0.28	1.10	0.89	1139	1.0
S70	246.86		38.21	3.84		0.25	1.74	1.37	2008	1.8
S71	433.35		49.18	6.42		0.26	3.06	2.28	3222	3.0
S72	460.77		82.91	4.61		0.30	3.25	1.64	3440	3.2
S73	564.70		147.63	2.55		0.36	3.99	0.91	4697	4.3
S74	744.36		153.98	2.94		0.31	5.26	1.05	5158	4.7
S75	853.55		196.26	2.37		0.32	6.03	0.84	6025	5.5
S76	982.97		295.72	4.54		0.35	6.87	1.62	8148	7.5
S77	325.30		72.43	2.63		0.32	2.30	0.94	2289	2.1
S78	396.49		77.21	2.70		0.31	2.80	0.96	3879	3.6
S79	574.60		99.76	3.09		0.32	4.06	1.10	4708	4.3
S80	690.89		160.98	3.47		0.34	4.88	1.24	5451	5.0
S81	169.86		38.23	3.02		0.27	1.20	1.07	1317	1.2
S82	260.72		39.36	4.61		0.27	1.84	1.64	2169	2.0
S83	401.81		51.43	4.20		0.26	2.84	1.50	2647	2.4
S84	473.23		87.67	4.94		0.29	3.34	1.76	3589	3.3

Specimen	P_u (kN)	P_y (kN)	P_{cr} (kN)	Δ_u (mm)	Δ_y (mm)	Δ_{cr} (mm)	Q_{uR}	α_{uR}	*I*	I_{uR}
S85	552.58		143.38	2.30		0.32	3.90	0.82	3252	3.0
S86	657.33		159.68	6.30		0.29	4.64	2.24	5226	4.8
S87	855.04		211.25	5.43		0.36	6.04	1.93	4052	3.7
S88	1091.01		262.26	3.22		0.29	7.70	1.15	4738	4.4
S89	307.32	192.59	76.99	2.40	4.66	0.3217	2.17	0.85	2017	1.9
S90	406.85	381.67	84.37	2.75	4.01	0.31	2.87	0.98	3574	3.3
S91	613.52	462.25	102.29	3.70	4.40	0.32	4.33	1.32	4266	3.9
S92	690.99	N.Y	164.68	3.37	N.Y	0.33	4.88	1.20	6088	5.6
S93	159.26	129.55	37.48	2.73	7.28	0.27	1.12	0.97	1203	1.1
S94	247.99	192.69	41.81	3.78	6.50	0.27	1.75	1.34	1920	1.8
S95	389.48	302.82	53.68	5.79	8.00	0.26	2.75	2.06	2914	2.7
S96	512.85	N.Y	85.62	5.08	N.Y	0.28	3.62	1.81	2074	1.9

**: The longitudinal steel in flange Did Not Yield*

Where:

Q_{uR} = Shear capacity ratio at the ultimate load level = P_u / P_{ur} (5)

α_{uR} = Deflection ratio at the ultimate load level = Δ_u / Δ_{ur} (7)

I_{uR} = Toughness ratio = I / I_{ur} (8)

And

P_{cr} : Cracked load (kN).
Δ_{cr} : The deflection at the first crack (mm).
P_{ur} : Shear capacity at the ultimate load level for the control specimen (S).
Δ_{ur} : Deflection at the ultimate level for the control specimen.
I_{ur} : Toughness of the control specimen.

4.3. Effect of flange dimensions: width ratio ($\rho_b = b_f/b_w$) and depth ratio ($\rho_t = t/h$)

Figure 11 presents the variation of beam ultimate shear strength, P_u, with the flange width ratio (ρ_b) for T-beams with variable flange thickness ratio (ρ_t). In addition, Fig. 12 presents the variation of beam ultimate shear strength, P_u, with the flange thickness ratio (ρ_t) for

T-beams with variable flange width ratio (ρ_b). The data in Figs. 11 and 12 corresponds to beams with ρ= 0.5, fc'= 30, and a/h= 2. Compared to control beam S (with P_u= 141.61 kN), presence of flange with a width of triple times web width (ρ_b= 3) and with thickness of 0.1, 0.3, 0.5, and 0.7 of beam depth; increased beam shear strength P_u by 10%, 40%, 90%, and 150%; respectively. Besides, for flange width of nine times web width (ρ_b= 9), the corresponding increases in beam shear strength become 12%, 75%, 175%, and 260%; respectively. Both flange width and thickness affects the shear strength of T-beams while the effect of flange thickness is more pronounced. For thin flanges (ρ_t= *0.10*), increasing flange width does not help.

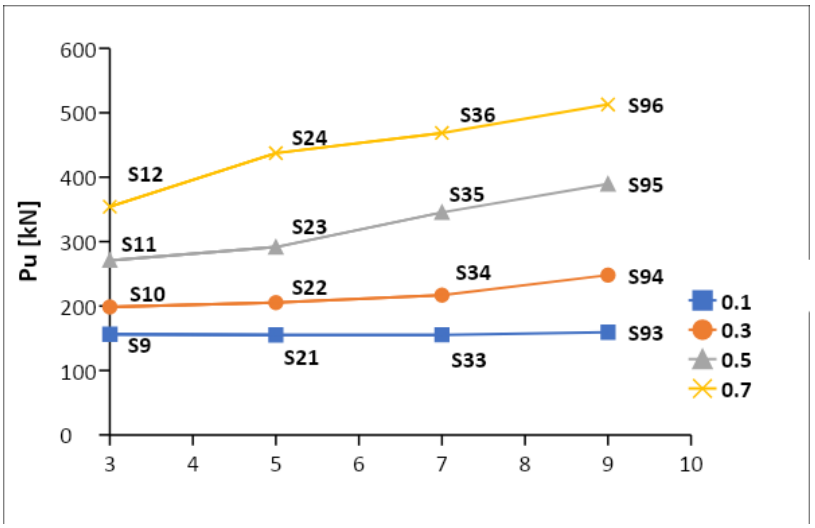

Fig. 11. Variation of ultimate load P_u with flange width ratio (ρ_b) at different flange thickness ratios (ρ_t) for *ρ= 0.5, fc'= 30* MPa & a/h= 2.

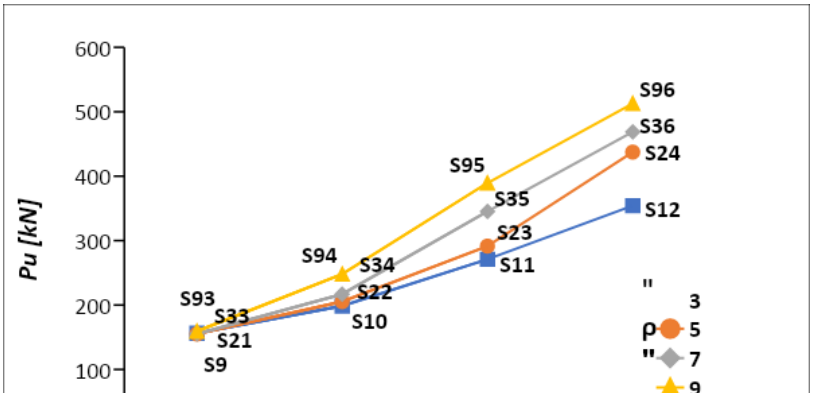

Fig. 12. Variation of ultimate load P_u with flange thickness ratio (ρ_t) at different flange width ratios (ρ_b) for ρ= *0.5, fc'= 30* MPa & a/h= 2.

4.4. Effect of longitudinal steel in flange

The ultimate load predicted for T-beams with variable flange longitudinal reinforcement percentile ratios (0, 0.5, 1.0, and 2) is shown in Fig.13 for three cases of shear span to depth ratio (*a/h*= 0.5, 1.0, and 2.0). This figure shows that increasing flange longitudinal reinforcement, ρ, from 0% to 2% increases the beam ultimate load by an average of 8%, 29%, and 27% for *a/h*= 0.5, 1.0, and 2; respectively.

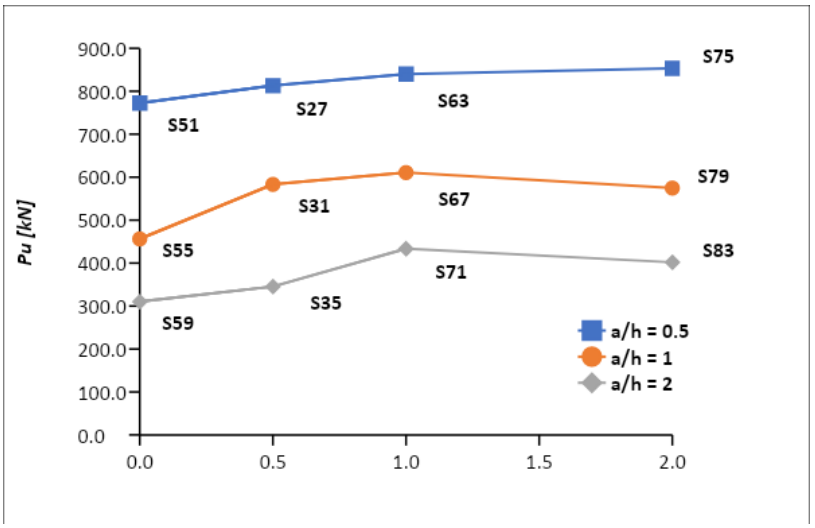

Fig. 13. Effect of flange longitudinal reinforcement on Ultimate load for different shear span to depth ratios for ρ_b *=7,* ρ_t *=0.5 &* fc' *=30* MPa.

4.5. Effect of shear span to depth ratio

Results for T-beams with different shear span to depth ratios (*a/h*= 0.5, 1, and 2) are shown in Figs. 14 and 15 for ρ_t *=0.3* and ρ *=0.5*.

Figure 14 presents variations of the ultimate shear strength with the shear span-to-depth ratio for ρ_b *=7* and two values of concrete characteristic strength (f_c*'= 30* MPa *and 60* MPa), ρ_t *=0.3,* ρ *=0.5)* and ρ_b *=7.* For *fc' =30* MPa, Fig. 15 depicts variations of the ultimate shear strength with the shear span-to-depth ratio at various flange widths (ρ_b *=3, 5, 7, & 9)*. The increase in (*a/h*) obviously reduced the shear capacity of flanged beams. In particular, decreasing the shear span to depth ratio from 2.0 to 1.0, and then to 0.5 increased the ultimate shear strength by an average of 49% and 120%, respectively. This trend is repeated for all flange widths and concrete strengths.

The load deflection curves for three T-beams that are identical, but have different shear span to depth ratios (*a/h= 0.5, 1.0, and 2.0*) are presented in Fig.16. The curve indicates that the beam toughness (I) is reduced as the shear span increases. Numerical values revealed that the toughness of beams having *a/h* of 1.0 and 2.0 were less than that of the similar beam with *a/h* of 0.5 by about 28% and 49%, respectively.

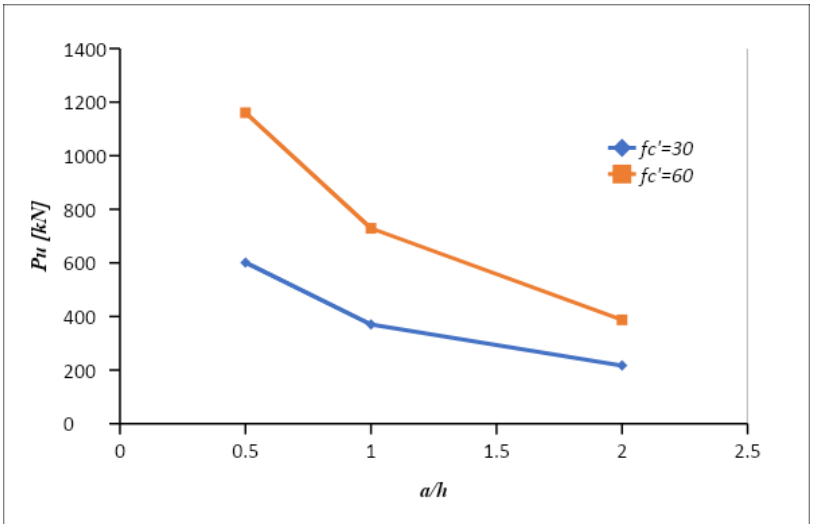

Fig. 14. Effect of shear span-to-depth ratio on ultimate shear strength of T-beams for two values of concrete characteristic strength *(ρ_b =7, ρ_t =0.3, ρ =0.5)* .

Fig. Effect of shear span-to-depth ratio on ultimate shear strength of T-beams with various flange widths (ρ_t *=0.3,* ρ *=0.5&* fc' *=30* MPa*).*

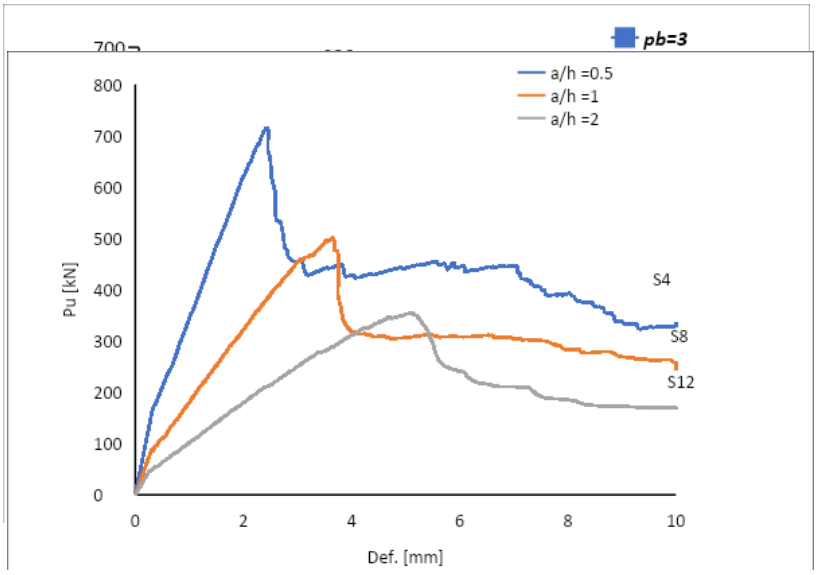

Fig. 16. Effect of shear span-to-depth ratio on load-deflection curves of flanged beams (ρ_b=3, ρ_t=0.7, fc'=30 MPa & ρ=0.5.

4.6. Effect of concrete characteristic strength.

Values of the ultimate shear strengths calculated for 24 T-beams are displayed in Fig. 17. These values correspond to T-beams with one flange width ρ_b=7; four values of flange thickness ρ_t=0.1, 0.3, 0.5 & 0.7; and two values of concrete characteristic strengths (fc'= 30 and 60MPa). Study of data in Fig.17 and Table 3 showed that- on average- doubling concrete strength of beams results in doubling the first-yield load and increases the first-crack load by about 20%. The increase in beam ultimate shear capacity varies with both shear span and flange thickness. Numerically, doubling fc' lead to shear capacity increases of 65%:99% for a/h =0.5; 54%:97% for a/h=1; and 27%:88% for a/h=2. It is also noted that the increase in

shear capacity with increasing concrete strength becomes less pronounced as the span length or the flange thickness increases.

To examine the effect of concrete characteristic strength on beam toughness, the load-deflection relationship for beams with *fc'*= 30 and 60MPa are presented in Fig. 18 for three flange thickness ratios ρ_t= 0.1, 0.3 &0.7 (other variables are ρ_b=7, *a/h*= 0.5). Considerable increase with an average of 74% in beam toughness, *I*, is observed with the increase in *fc'* from 30 to 60 MPa. Finally, Fig.19 shows that the flexural crack pattern at failure is similar for beams with concrete strength of 30 to 60 MPa, while the use of higher concrete strength delayed the premature shear failure.

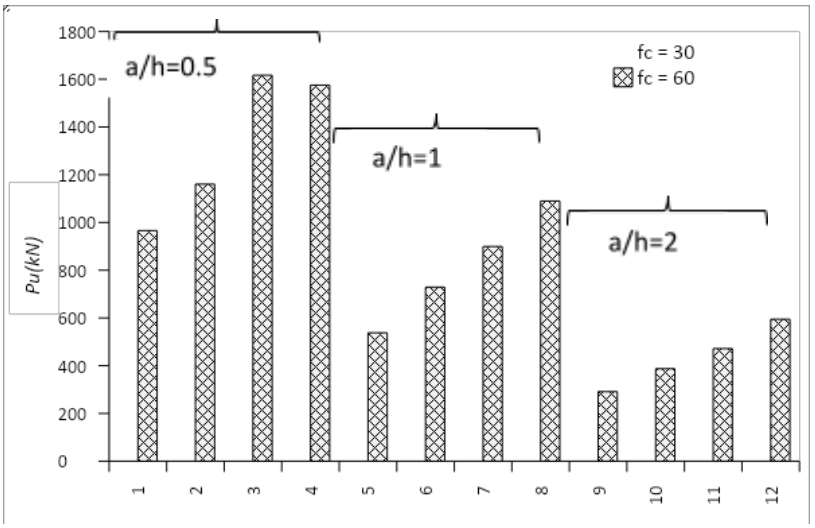

Fig. 17. Effect of concrete characteristic strength on shear capacity for beams with variable shear span to depth ratios (ρ_b=7, ρ_t= 0.1, 0.3, 0.5& 0.7).

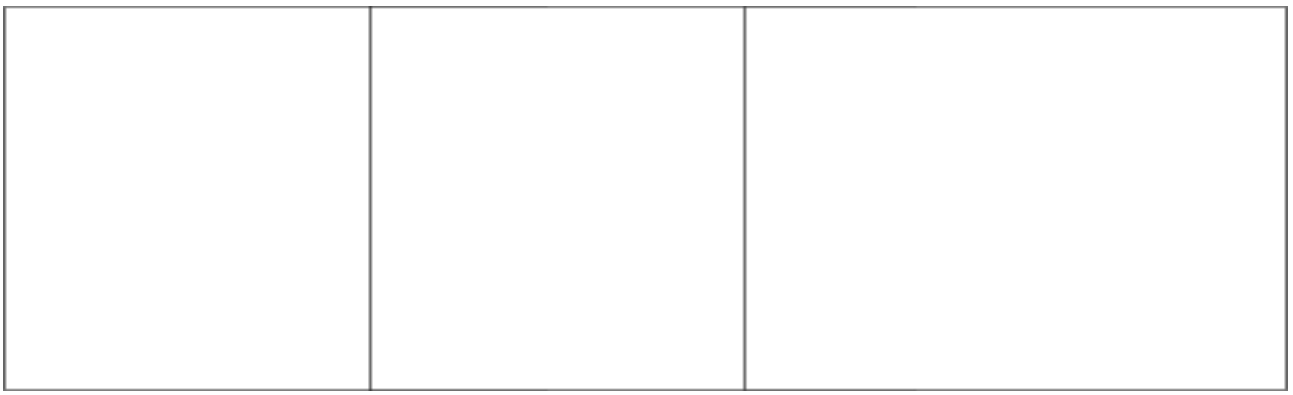

ρ_t= 0.1 ρ_t= 0.3 ρ_t= 0.7

Fig. 18. Effect of concrete characteristic strength on load-deflection relationship for beams with variable flange thickness (ρ_b=7, *a/h*= 0.5).

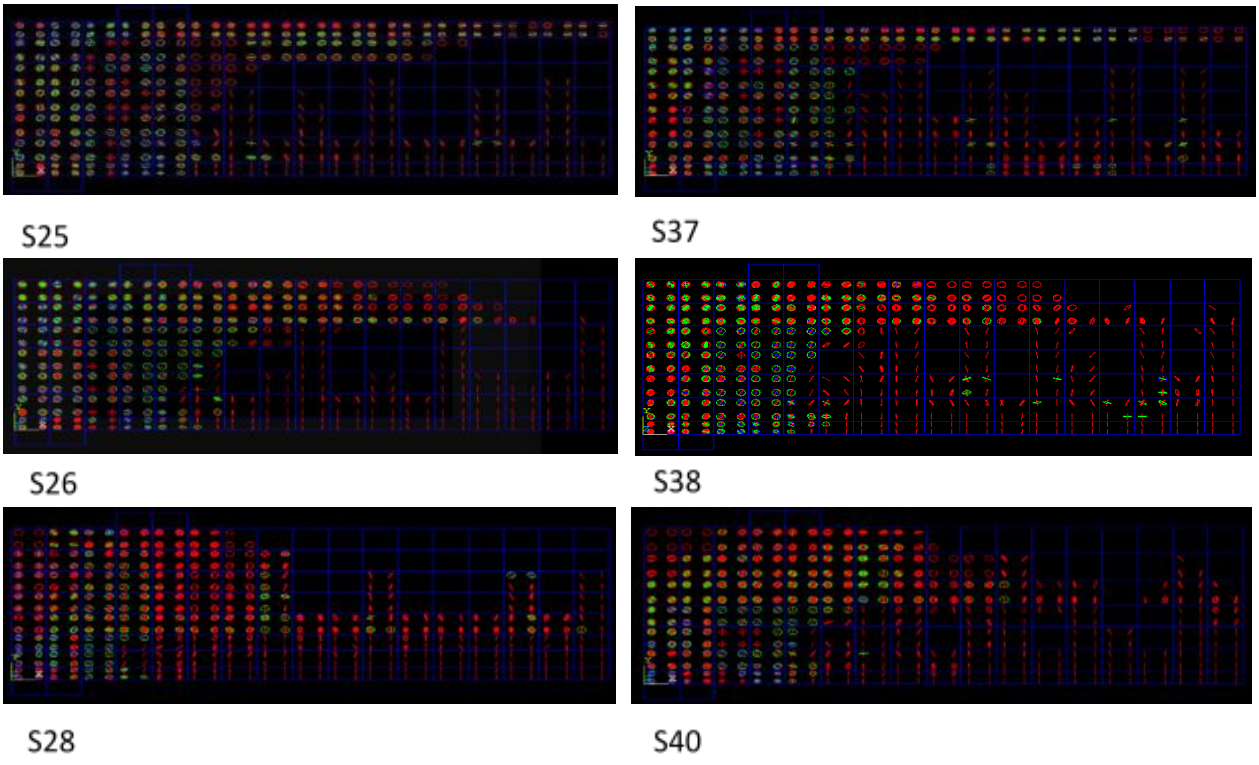

(a) *fc'*= 30 MPa **(b)** *fc'*= 60 MPa

Fig. 19. Effect of concrete characteristic strength on crack patterns at failure for beams with variable flange thickness: ρ_t= 0.1 for S25&37, 0.3 for S26&38, 0.7 for S28&40 (ρ_b=7, a/d= 0.5 & ρ= *0.5*%).

5. Conclusions

The following remarks are derived based on the ANSYS finite element results of the validated model:

1. Good general agreement is observed between the results of the developed nonlinear FE model (by ANSYS) and the corresponding experimental results in terms of load-deflection relationships, crack patterns and propagation history, and failure modes. The average value of the ultimate load ratios ($P_{u(FE)}/P_{u(EXP)}$) and ultimate deflection ratios ($\Delta_{u(FE)}/\Delta_{u(EXP)}$) was 1.03 and 0.87, respectively.
2. The most important parameters in improving the shear capacity of T-beams are the ratio of flange thickness to beam depth (t/h) followed by the ratio of flange width to web width (b_f/b_w). Presence of flange with (t/h) = 0.1 to 0.7 increased the shear strength P_u by 10% to 150% for (b_f/b_w) = 3 and by 12% to 260% for (b_f/b_w) = 9. Thus, the effect of flange thickness is more pronounced. For thin flanges ($t/h = 0.10$), increasing flange width does not help.
3. Increasing flange longitudinal reinforcement, ρ, from 0% to 2% increased the beam ultimate load by an average of 8%, 29%, and 27% for shear span to depth ratio *(a/h)* of 0.5, 1.0, and 2; respectively.
4. Investigation of the load deflection curves for identical T-beams that have different shear spans indicated that the beam toughness (I) decreases as the shear span increases. In particular, the toughness of beams with *a/h* of 1.0 and 2.0 were less than that of the similar beam with *a/h* of 0.5 by about 28% and 49%, respectively.
5. Increasing the concrete characteristic strength *fc'* from 30 to 60 MPa increased the beam shear capacity by 65%:99% for *a/h* =0.5; 54%:97% for *a/h*=1; and 27%:88% for *a/h*=2.

6. The results of this study contribute to reduced projects' cost, by the contribution of the thick flange in the compression zone, when it is taken into consideration and not neglected in the design of flange beams.

References

[1] ANSYS-Release Version 19.2.0., "A Finite Element Computer Software and User Manual for Nonlinear Structural Analysis," ANSYS Inc. Canonsburg, PA 15317, 2018.

[2] Hesham A. A. and Wael M. M., "Shear behavior of reinforced lightweight concrete T-beams," Life Science Journal, 16(8), 2019.

[3] Balamuralikrishnan R. and Saravanan J., "Finite Element Modelling of RC T - Beams Reinforced Internally with GFRP Reinforcements," Civil Engineering Journal, 5(3), 2019.

[4] Hamdy K. S., Mohamed M. H., Mahmoud A. K. and Mahmoud Y. A. Z. "Finite Element Analysis on the behavior of Strengthened RC Shallow T-Beams with Large Openings at Shear Zone Using CFRP and BFRP sheets," IJSEAS, 3(11), 2017.

[5] Hugo C. B., Carlos C. and Manuel A.G., "A smeared Crack Analysis of Reinforced Concrete T-Beams Strengthened with GFRP Composites," Engineering Structures 56, 2013: 1346-1361.

[6] Pansuk W and Sato Y., "Shear Mechanism Of Reinforcement Concrete T-Beams With Stirrups," Journal of Advanced Concrete Technology, 5(3), 2007: 395-408.

[7] Pansuk W., Sato Y., Takahashi R. and Ueda T., "Influence of Top Flange to Shear Capacity of Reinforced Concrete T-Beams," Concrete Engineering Annual Papers, 26(2), 2004.

[8] Giaccio C., Al-Mahaidi R, and Taplin G., "Experimental study on the effect of flange geometry on the shear strength of reinforced concrete T-beams subjected to concentrated loads," Can. J. Civ. Eng. 29,2002: 911-918

[9] Kachlakev D., and Miller T., "Finite Element Modeling of Reinforced Concrete Structures Strengthened with FRP Laminates," Final Report, Oregon Department of Transportation, Salem, Oregon, May 2001.

[10] Musmar M. A., Rjoub M. I. and Abdel Hadi M. A., "Nonlinear Finite Element Analysis of Shallow Reinforced Concrete Beams Using SOLID65 Element," ARPN Journal of Engineering and Applied Sciences, 9(2), February 2014: 85-89

[11] Tjitradi D., Eliatun E. and Taufik S., "3D ANSYS Numerical Modeling of Reinforced Concrete Beam Behavior under Different Collapsed Mechanisms," International Journal of Mechanics and Applications 2017, 7(1): 14-23

[12] Shah, S. P., Swartz, S. E., and Ouyang, C., "Fracture Mechanics of Concrete," John Wiley & Sons, Inc., New York, 1995.

[13] Bangash, M. Y. H., “Concrete and Concrete Structures: Numerical Modeling and Applications,” Elsevier Science Publishers Ltd., London, England, 1989.

[14] Gere, J. M. and Timoshenko, S. P.,” Mechanics of Materials,” PWS Publishing Company, Boston, Massachusetts, 1997.

[15] Kachlakev, D.I. and McCurry, D., Jr., “Simulated Full Scale Testing of Reinforced Concrete Beams Strengthened with FRP Composites: Experimental Results and Design Model Verification,” Oregon Department of Transportation, Salem, Oregon, June 2000.

[16] Ramadan, O. M., Abdel-Kareem, A. H., El-Azab, I. A., & Abousafa, H. R.,” Flange Contribution to the Shear Strength of RC T-Beams with Flange in Compression”. Buildings 2022, 12(6): 803.

[17] ACI Committee 318.,” Building Code Requirements for Structural Concrete ACI,” vols. 318-14, 2014.